Rapid blazar flares for ASTRI and CTAO

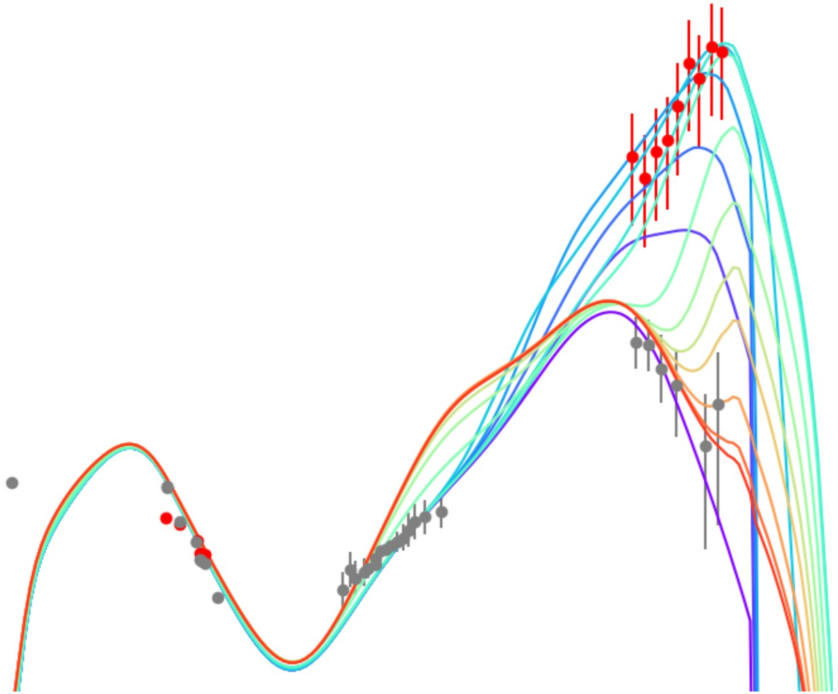

A. Zech

"From nine to forty" workshop at Sexten
July 2026

LUX Observatoire de Paris | PSL

emission of different blazar types

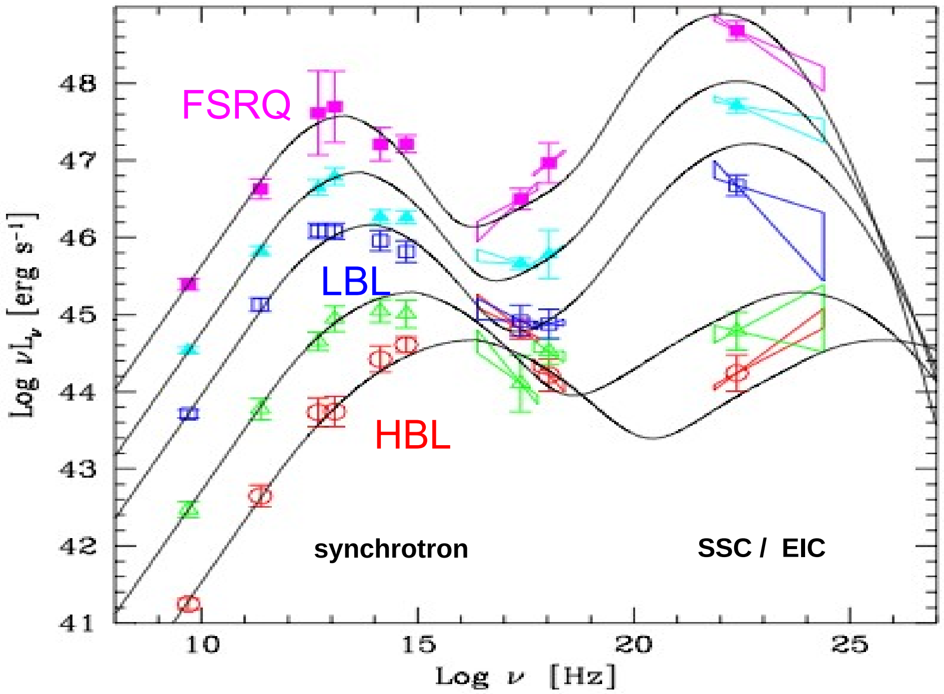

Donato et al. (2002), based on Fossati et al. (1998)

luminous **FSRQs** with low peak energies
↔ less luminous **BL Lac objects** with high peak energies

emission of different blazar types

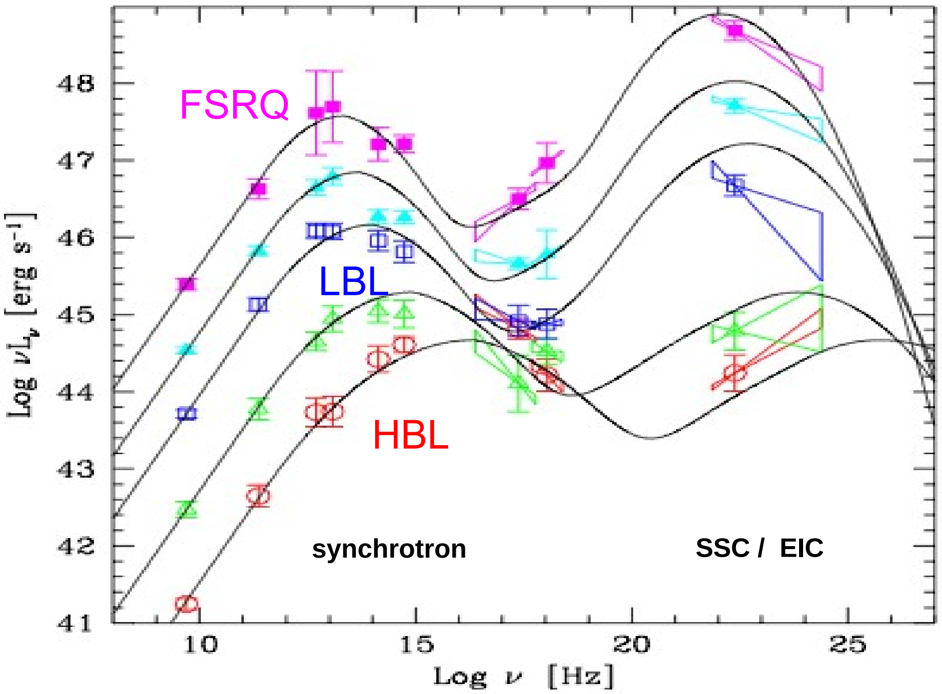

Donato et al. (2002), based on Fossati et al. (1998)

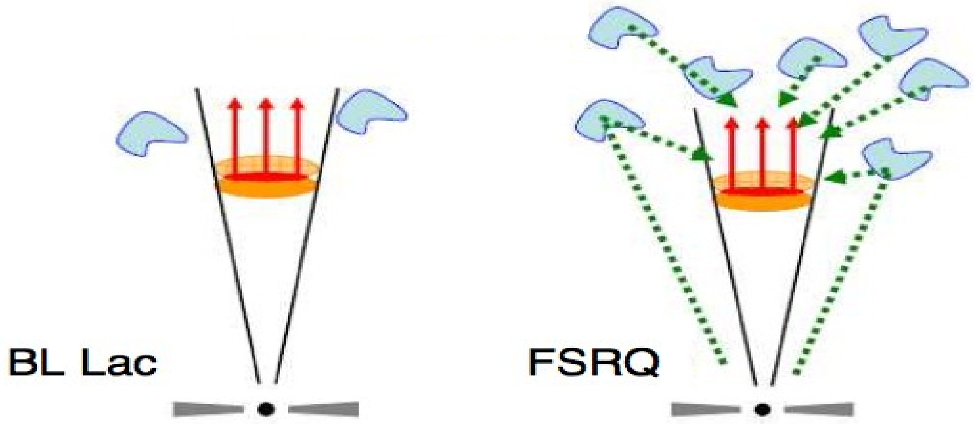

B. Lott, Cospar 02/10

luminous **FSRQs** with low peak energies
↔ less luminous **BL Lac objects** with high peak energies

- Disk, Broad Line Region, dust torus emit **weakly**

- leptonic models : γ-rays due to **Synchrotron Self Compton**

- Disk, Broad Line Region, dust torus emit **strongly**

- leptonic models: γ-rays mostly due to **External Inverse Compton**

flares from propagation through photon fields

(application to FSRQs)

Journal of High Energy Astrophysics 53 (2026) 100629

Contents lists available at ScienceDirect

Journal of High Energy Astrophysics

journal homepage: www.elsevier.com/locate/jheap

ELSEVIER

Check for updates

Blazar flares from plasma blobs crossing the broad-line region

S. Le Bihan [a,*], A. Dmytriiev [b], A. Zech [c]

[a] *Université Paris Cité, CNRS, Astroparticule et Cosmologie, Paris, F-75013, France*
[b] *Centre for Space Research, North-West University, Potchefstroom, 2520, South Africa*
[c] *LUX, Observatoire de Paris, Université PSL, Sorbonne Université, CNRS, Meudon, 92190, France*

an orphan flare from 3C 279 in 2013 ?

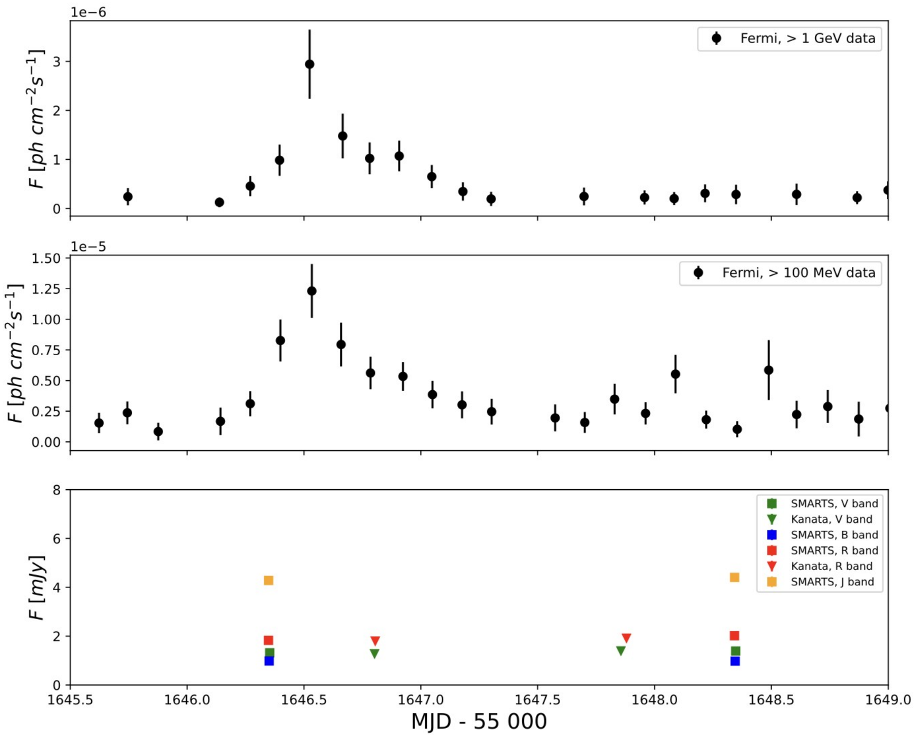

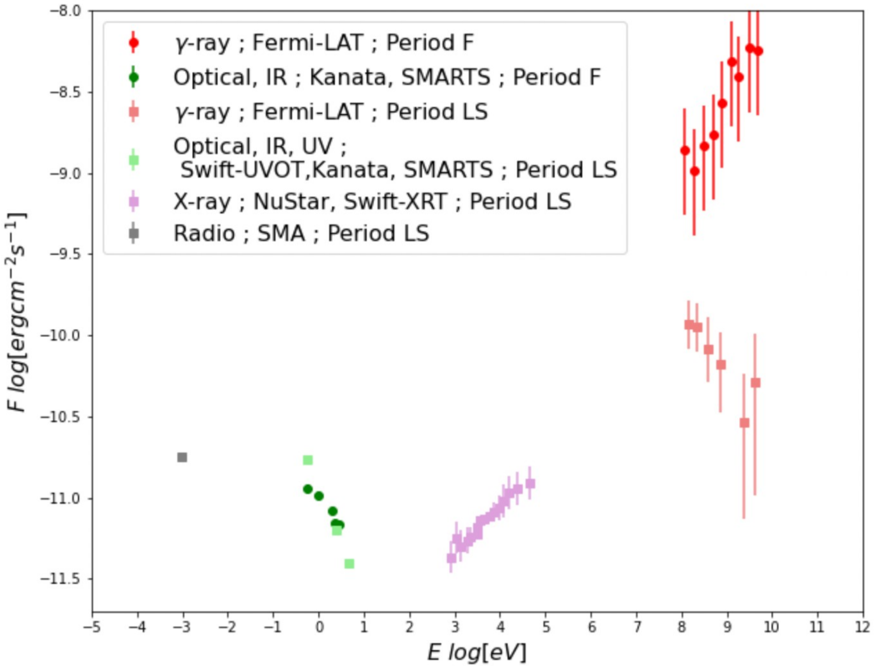

Le Bihan, Dmytriiev, Zech 2026;
with data from Hayashida et al. 2015

- significant Fermi flare from this FSRQ on 20.12.2013
- no significant variability in optical data
- no simultaneous X-ray data

modeling the photon fields in a FSRQ

- External Compton emission on photon fields from accretion disk, corona, Broad Line Region, dust torus

- In many scenarios, the **BLR** has the most significant contribution (emission region at sub-pc scales) :

  -- photons from a spectrum of emission lines

  -- BLR modeled as a spherical shell with inner radius R_{BLR} ~ 0.1 pc

  -- For distance d > R_{BLR}, the energy density decreases as :

$$U'(\epsilon', d) = \frac{L'_{BLR}(\epsilon')\Gamma^2_{blob}}{3\pi R^2_{BLR} c \left(1 + (d/R_{BLR})^{\beta_{BLR}}\right)}$$

(Hayashida et al 2012)

  -- γ-γ absorption following *Böttcher & Els (2016)*

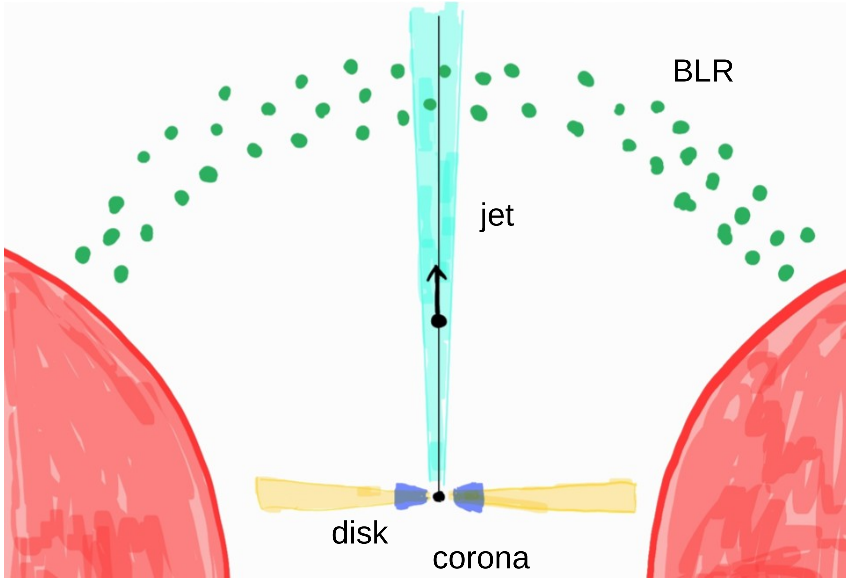

accelerating blob model

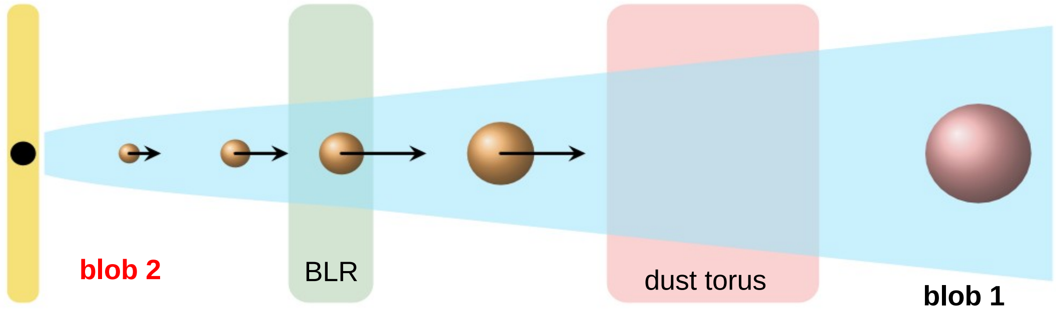

low-state emission from a stationary emission region, e.g. recollimation shock ("**blob 1**")

flare is caused by an accelerating, expanding emission region ("**blob 2**")

→ acceleration through differential collimation up to ~ BLR

$$\Gamma_{blob} = min\left(\Gamma_{max}, \sqrt{d/(3R_s)}\right)$$

Γ_{max} = 30

- for d < R_{BLR} , as blob 2 accelerates :

$$U' \propto d$$

- for d > d_{max}, as blob 2 advances at constant velocity :

$$U' \propto d^{-\beta_{BLR}}$$

Photon fields

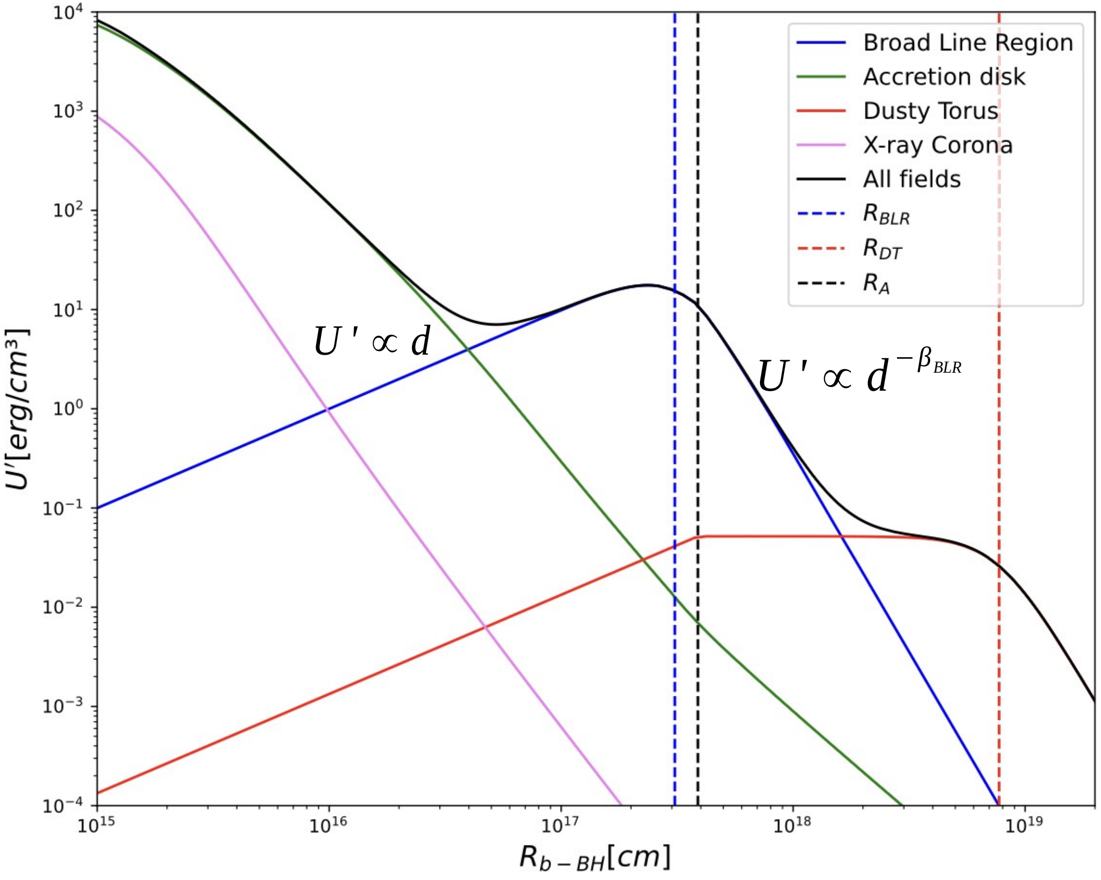

= “d”

Photon energy density **in the “blob” frame** vs. distance from black hole for an accelerating blob.

Time-dependent broad-band spectrum

Low-state SED from 'blob 1'

Flare is caused by 'blob 2'

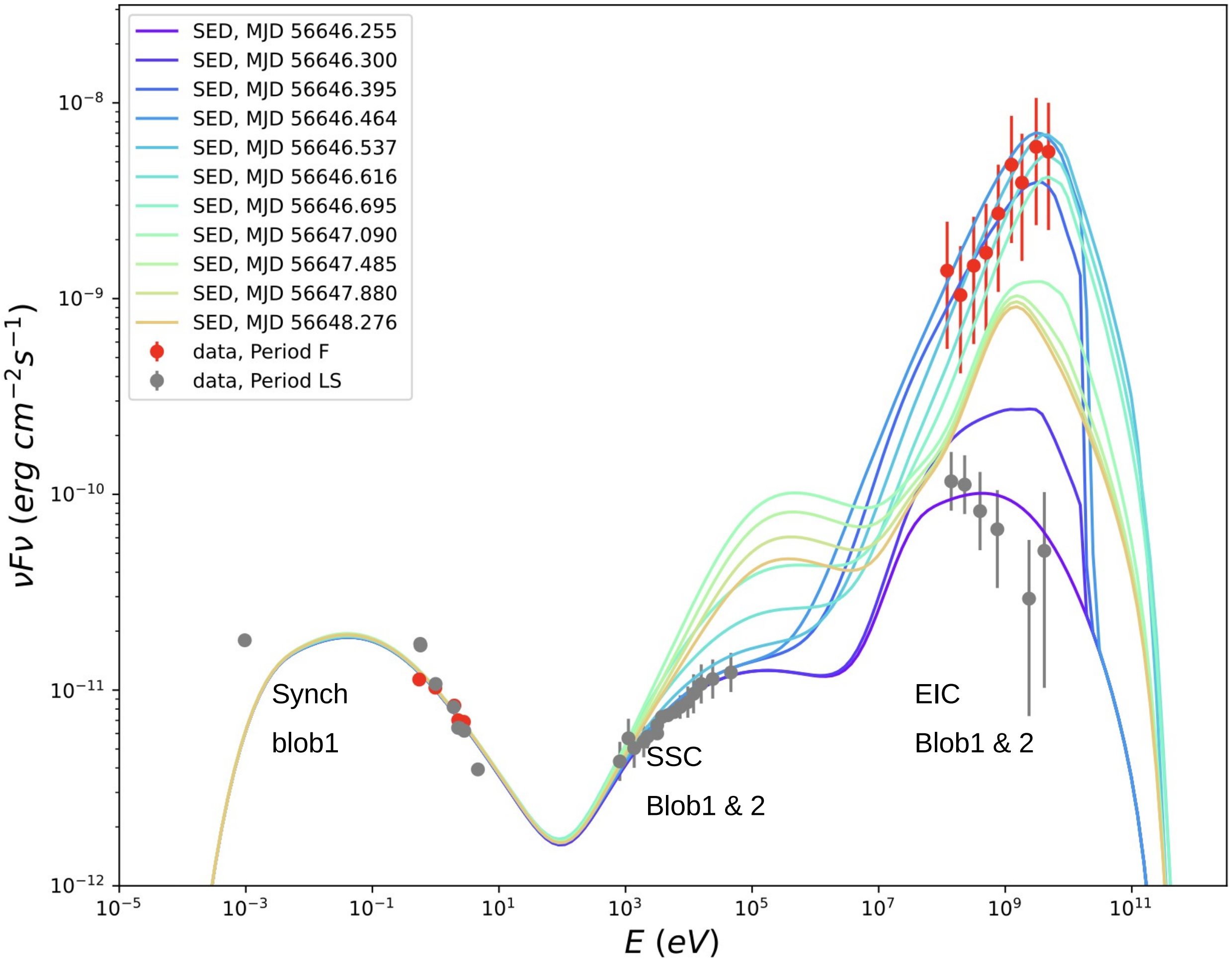

Multi-wavelength light curves

VHE band : delayed wrt HE band due to γγ pair production on the BLR photons

X-ray band : delayed wrt HE band due to a slower onset of the synchrotron emission from the moving blob
Emission is dominated by EIC (HE, VHE) before SSC flux (X-rays) rises above the low state flux

Optical band : no variation of the optical flux (by design)
The low-state flux always dominates in this band.

→ high-energy “orphan” flare

VHE

HE

X-ray

optical

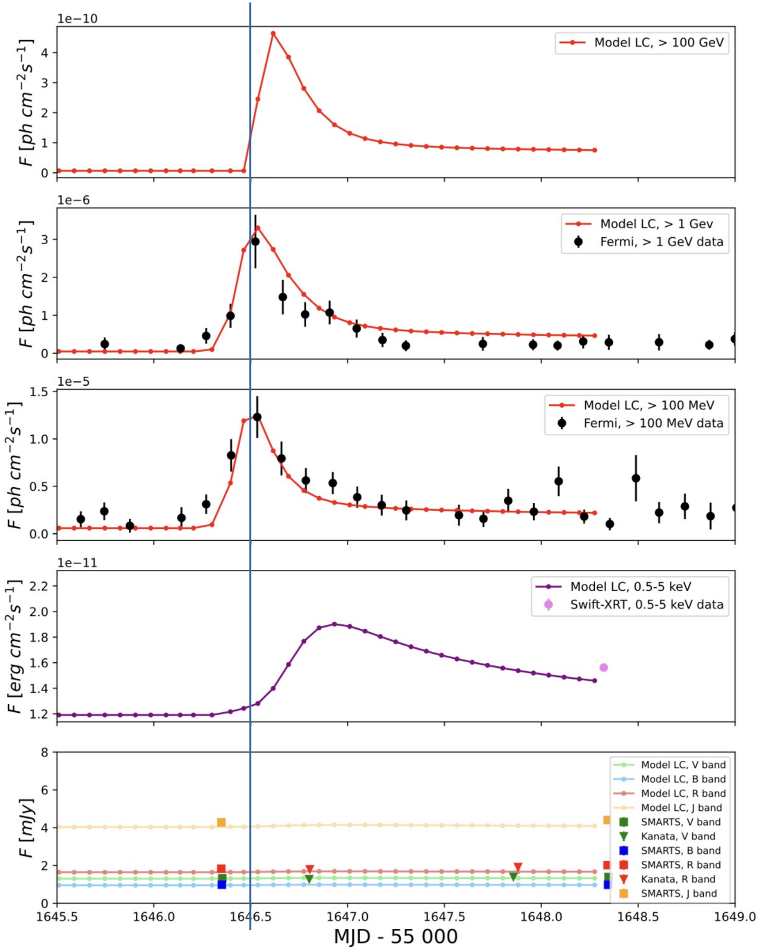

FSRQ flare sources for ASTRI and SSTs ?

some FSRQs to target for VHE flares :

3C 279 , *PKS 0736+017*, *PKS 1441+252*, *PKS 1510-089* , *PKS 1222+216*.
Ton 599, S3 0218+35

→ steep intrinsic spectra and γγ absorption on BLR and EBL
→ VHE data cut off below 1 TeV
→ targets for CTAO LSTs and MSTs

PKS 0903 – 57 : spectrum extends beyond 1 TeV !

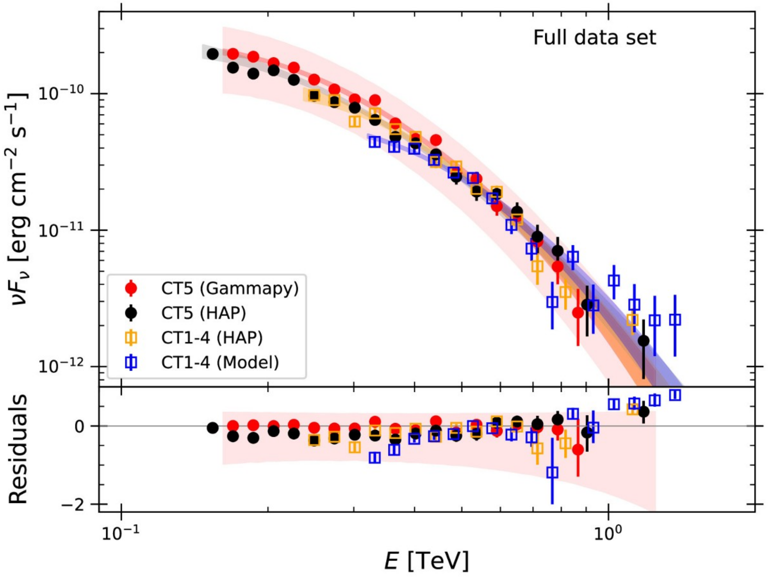

Acharyya et al. (H.E.S.S. Collab.)
JHEAp 53 (2026) 100599

flares from particle injection / acceleration

(here applied to BL Lacs)

A&A, 707, A288 (2026)
https://doi.org/10.1051/0004-6361/202554153

Astronomy & Astrophysics

Particle acceleration signatures in the time-dependent one-zone synchrotron self-Compton model of blazar flares

Paloma Thevenet[1,★], Andreas Zech[1,★], Catherine Boisson[1], and Anton Dmytriiev[2]

[1] LUX, Observatoire de Paris, Université PSL, CNRS, Sorbonne Université, 92190 Meudon, France
[2] Centre for Space Research, North-West University, Potchefstroom 2520, South Africa

Received 17 February 2025 / Accepted 22 January 2026

particle evolution through injection or acceleration

- flares arise from a change in the electron distribution in the emission zone
- particle distribution described by Fokker-Planck equation (e.g. EMBLEM code) :

Cooling terms — Acceleration terms

$$\frac{\partial N_e(\gamma,t)}{\partial t} = \frac{\partial}{\partial \gamma}[(b_c(\gamma,t)\gamma^2 + \frac{1}{t_{ad}}\gamma - a(t)\gamma - \frac{2}{\gamma}D_{F_{II}}(\gamma,t))N_e(\gamma,t)] + \frac{\partial}{\partial \gamma}\left(D_{F_{II}}(\gamma,t)\frac{\partial N_e(\gamma,t)}{\partial \gamma}\right)$$
$$- N_e(\gamma,t)\left(\frac{1}{t_{esc}} + \frac{3}{t_{ad}}\right) + \dot{Q}_{inj}(\gamma,t)$$

Injection term

Cooling

- Synchrotron and Inverse Compton: $b_c(\gamma,t) = \frac{4\sigma_T(u_B+u_{rad})}{3 m_e c}$
- Adiabatic expansion: $t_{ad}(t) = \frac{R(t)}{\beta_{exp} c}$

acceleration (of cold electrons)

Fermi I : Q_{inj}
Fermi II : $D_{FII} = p^2 / t_{FII}$

re-acceleration (of relativistic electrons)

Fermi I : $a = 1 / t_{shock}$
Fermi II : $D_{FII} = p^2 / t_{FII}$

e.g. Fermi-I acceleration

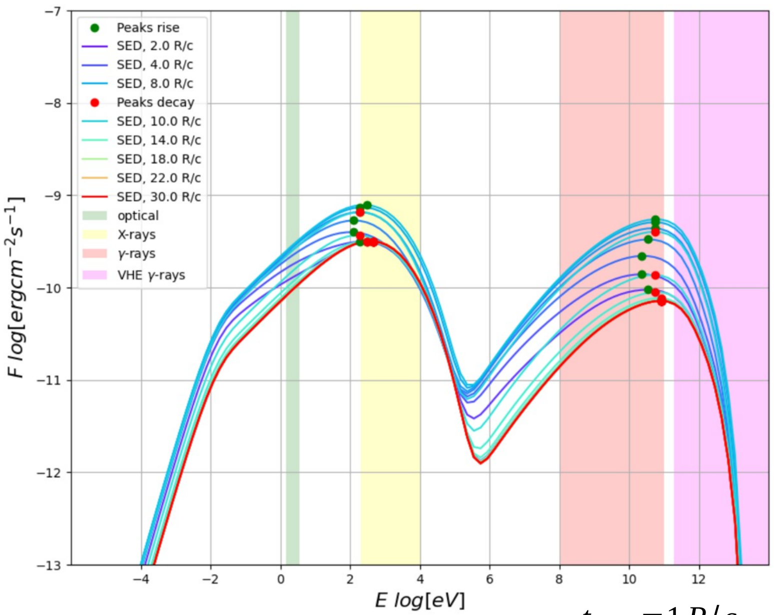

$t_{shock} = 1\, R/c$

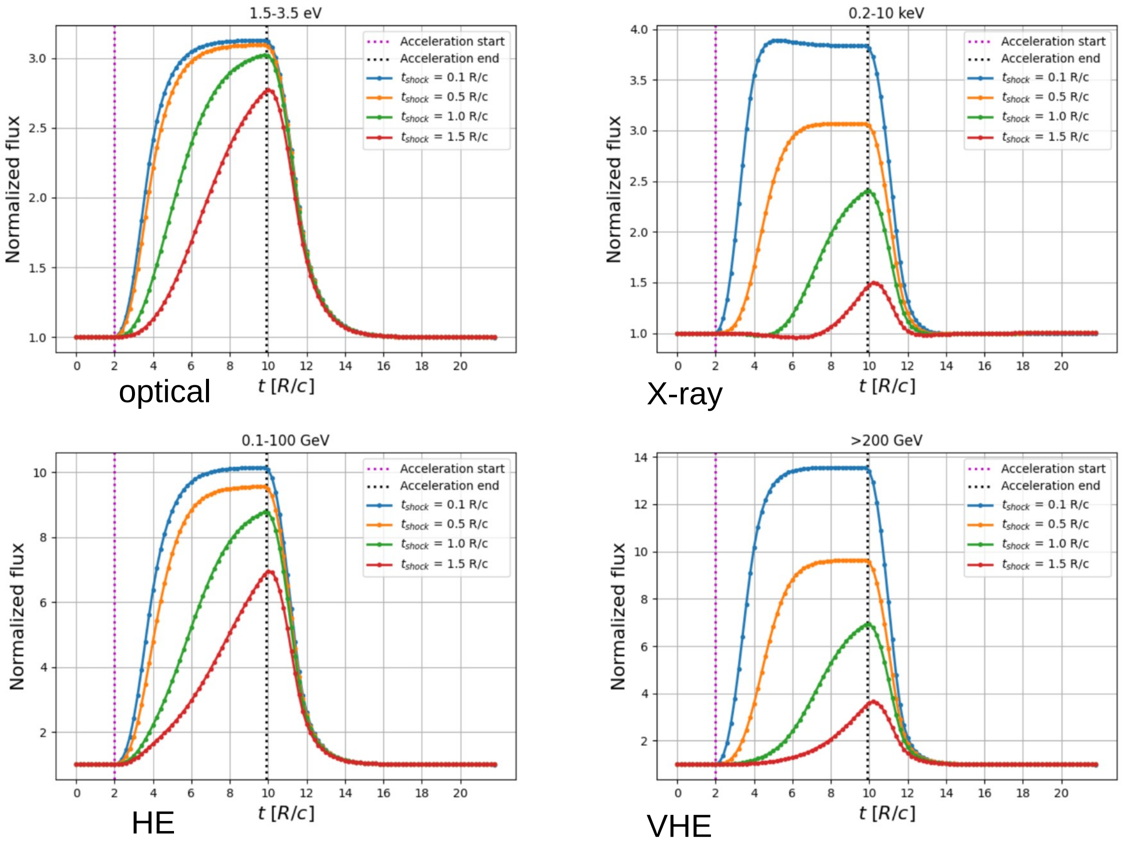

- shift of peaks during flare

- flare **onset** shifts between energy bands

- occurrence of a plateau
  (= high steady-state) only for very rapid t_{shock}

comparison with a 2013 flare of Mrk 421

- one single zone is not sufficient to describe the MWL behaviour
→ addition of a **baseline flux** to model the unknown continuum flux below the flare

- R/δ constrained by flare rise.
Escape time scale constrained by flare decay.

- for this simplified application, the injection scenario (= very efficient Fermi-I acceleration) provides the best representation of the high-energy data. Fermi I re-acceleration would require a second flare component.
Fermi II re-acceleration not compatible with X-ray flare shape in this case.

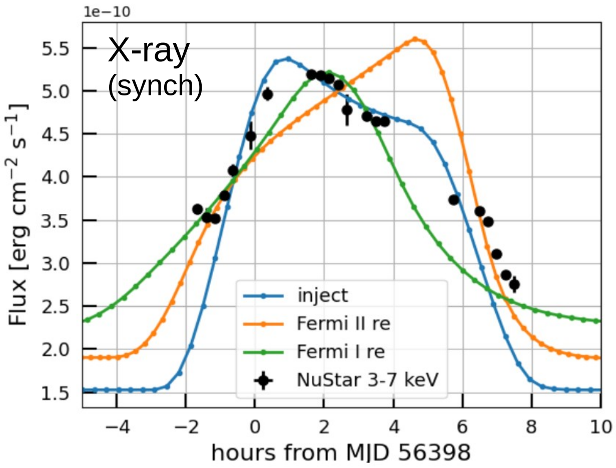

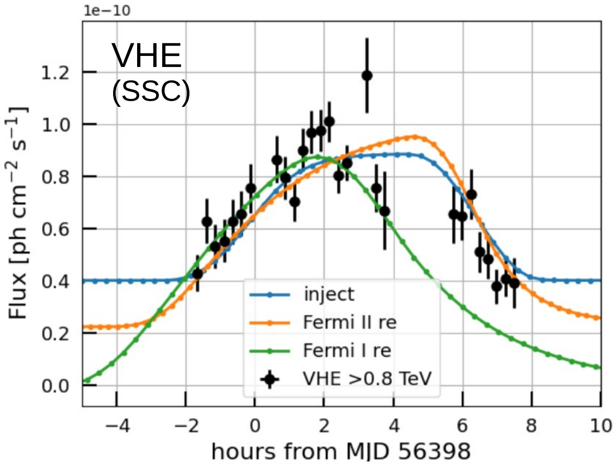

What would CTAO see ?

CTAO
Nord
(alpha)

Caveat:
10h of obs.
assumed

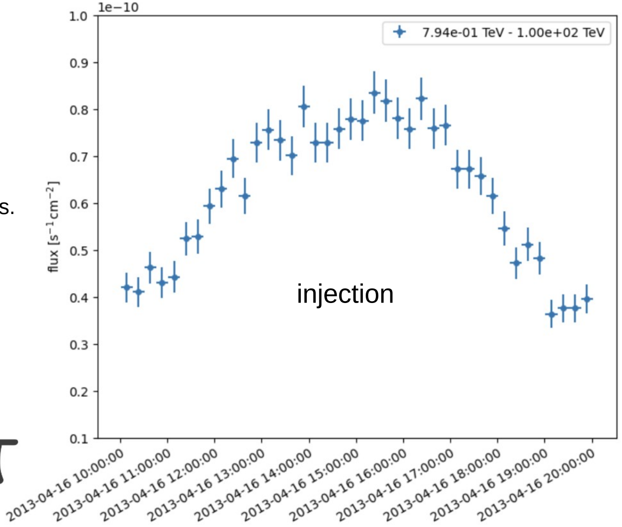

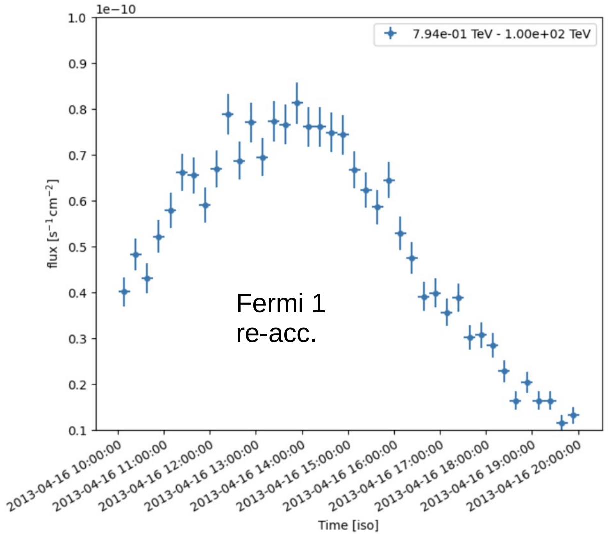

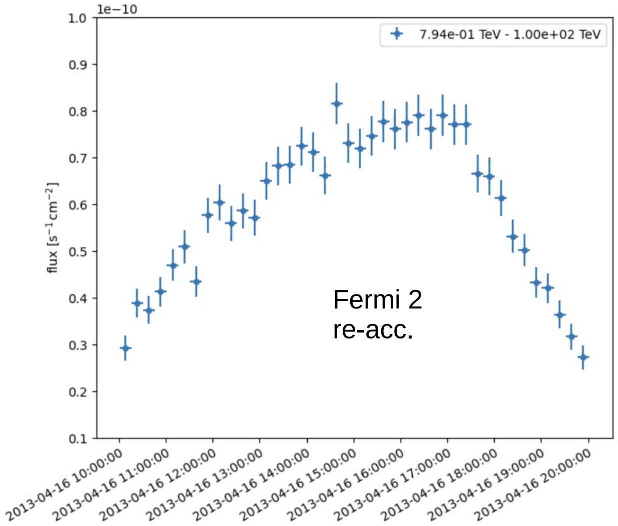

CTAO
Sud
(alpha)

Caveat:
10h of ob
assumed

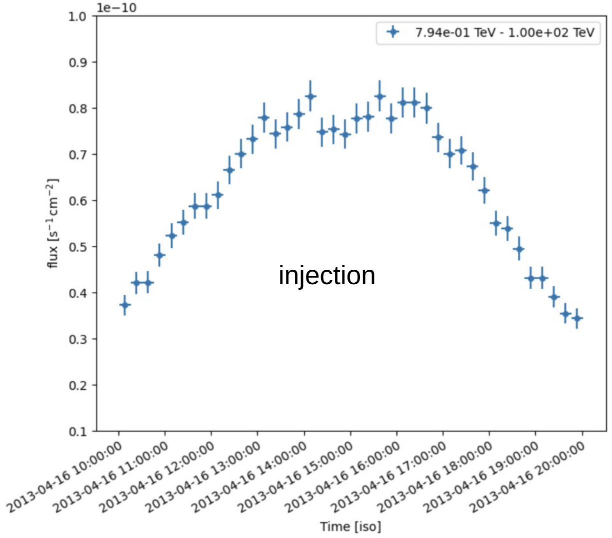

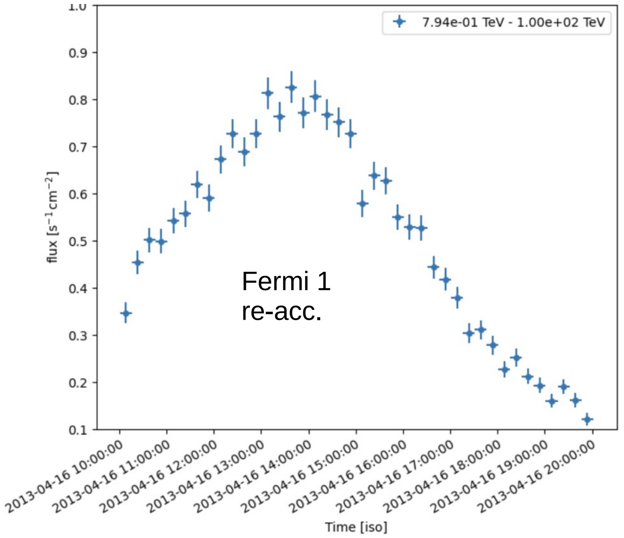

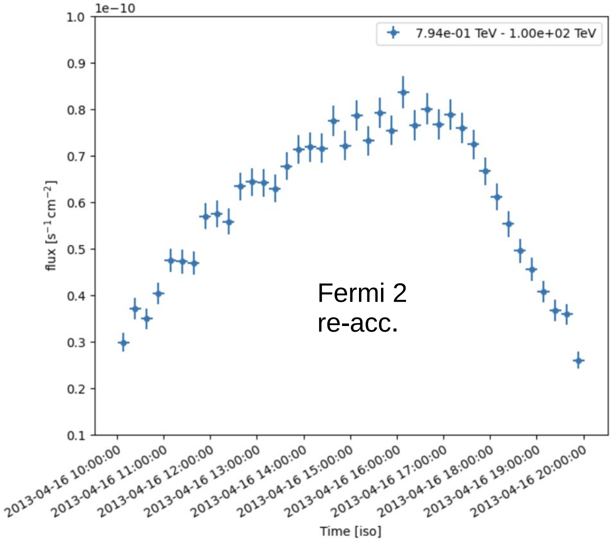

BL Lac flare sources for ASTRI and SSTs ?

Some BL Lac / FR I sources to watch out for **VHE flares at the highest energies** :

Mrk 421 : spectrum during 2010 flare extends beyond 10 TeV, detected by ASTRI-1 and SST-1M

Mrk 501 : spectrum observed up to 20 TeV

M87 : spectrum observed up to 20 TeV

PKS 2155-304 : frequent and spectacular flares, spectrum observed up to ~5 TeV

1ES 1727+502 : VHE flaring detected with LHAASO > 1 TeV in 2024

1ES 1426+428 : elevated state detected by VERITAS in 2021, spectrum extends >1 Tev

VER J0521+211 : large flare detected by VERITAS in 2020, spectrum extends >1 Tev

BL Lacertae : bright flare detected by LST-1 in 2022, spectrum extends >1 Tev
...

Conclusions

The temporal and spectral evolution of **rapid flares** can yield significant constraints on the particle acceleration and emission mechanisms.

Many more sophisticated models exist (reconnection in different regions, internal shocks and recollimation shocks, clouds crossing the jet, particle acceleration in the black hole magnetosphere…). Important to **extract basic observables** to distinguish between them.

ASTRI and the SSTs are well situated to target high-frequency peaked BL Lacs, but also M87, certain FSRQs.

Important to complement observation campaigns with simultaneous MWL (and MM) information.

flares : macroscopic vs. microscopic variations

variation of the macroscopic parameters of the emission region

- change in size of emission region R (expansion, contraction) or density
- change in magnetic field B or external radiation field
- change in Doppler beaming (Lorentz factor, viewing angle)

variation in the energy distribution of the emitting particles

- particle injection (pre-accelerated particle distribution)
- particle acceleration (shock, turbulence, magnetic reconnection...)

accelerating blob model

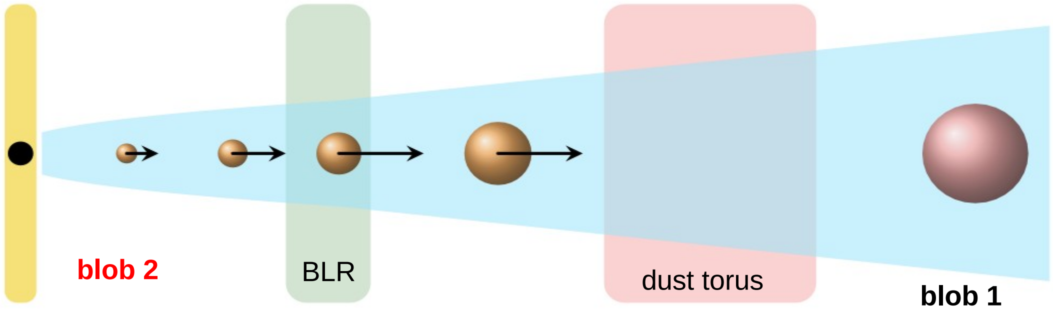

B'_{blob1} = 0.09 G , initial B'_{blob2} = 0.03 G ,
R'_{blob1} ~ 5 x 10^{16} cm, initial R'_{blob2} ~ 2 x 10^{15} cm

particle spectrum

- continuous injection of a steep power-law
(bow shock ? turbulent acceleration ? reconnection ?)

- cooling (adiabatic, synchrotron, Inverse Compton)

- particle escape

relativistic effects important for BLR crossing !

Distance traveled in observed time interval Δt_{obs} :

$$D = \Delta t_{obs} \beta_{blob} c \delta \Gamma_{blob} / (1+z)$$

Electron evolution

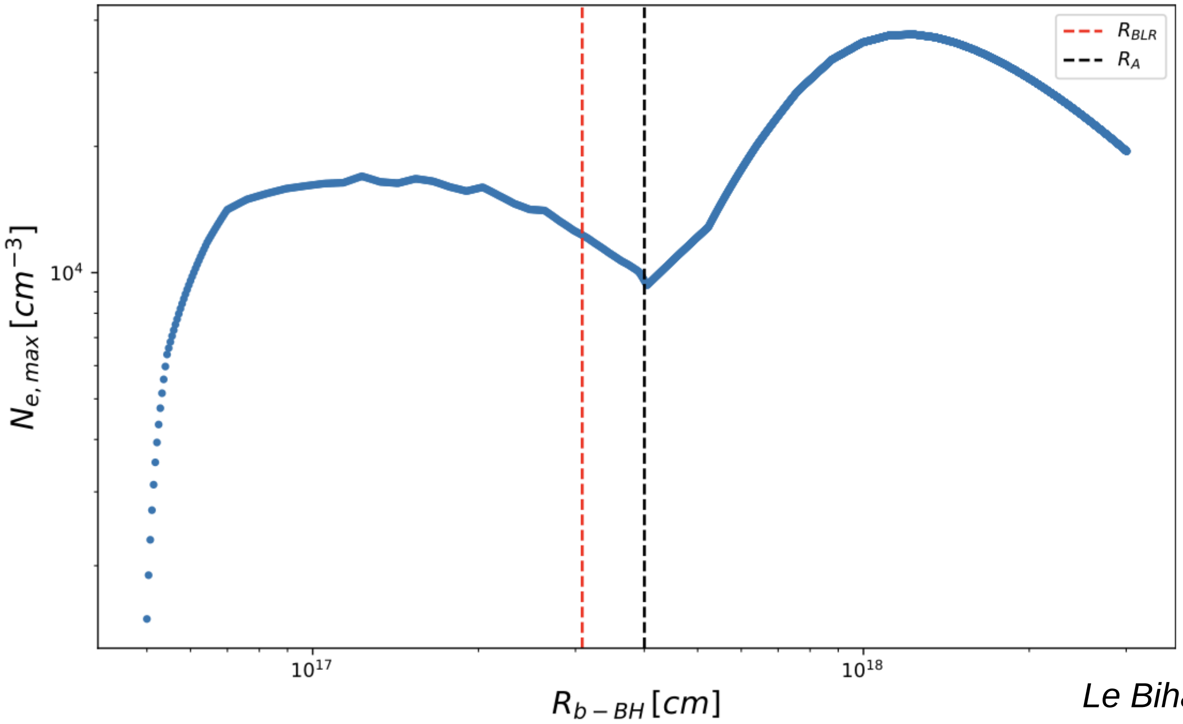

Le Bihan, Dmytriiev, AZ, 2026

Fig. C.4. Maximum of the electron distribution of blob 2 as a function of distance to the black hole.

Accelerating blob, model parameters

Parameter	Blob 1	Blob 2
Blob characteristics		
Type	Stationary	Accelerating
B(G)	0.09	[0.03,0.02]
R_{b-BH}(cm)	2.0×10^{19}	$[0.05, 3] \times 10^{18}$
R_b(cm)	5.0×10^{16}	$[2.0, 2.9] \times 10^{15}$
Injection spectrum		
Type	BPL	PL
$N(\mathrm{cm}^{-3}\mathrm{s}^{-1})$	3.0×10^{-7}	5.0×10^{-1}
γ_{pvt}	215	200
γ_{brk}	3000	/
α_1	−2.5	/
α_2	−3.5	−3.5
$\gamma_{\min}$	200	1300
$\gamma_{\max}$	10^5	10^5

Accelerating blob, impact of the length of acc. region

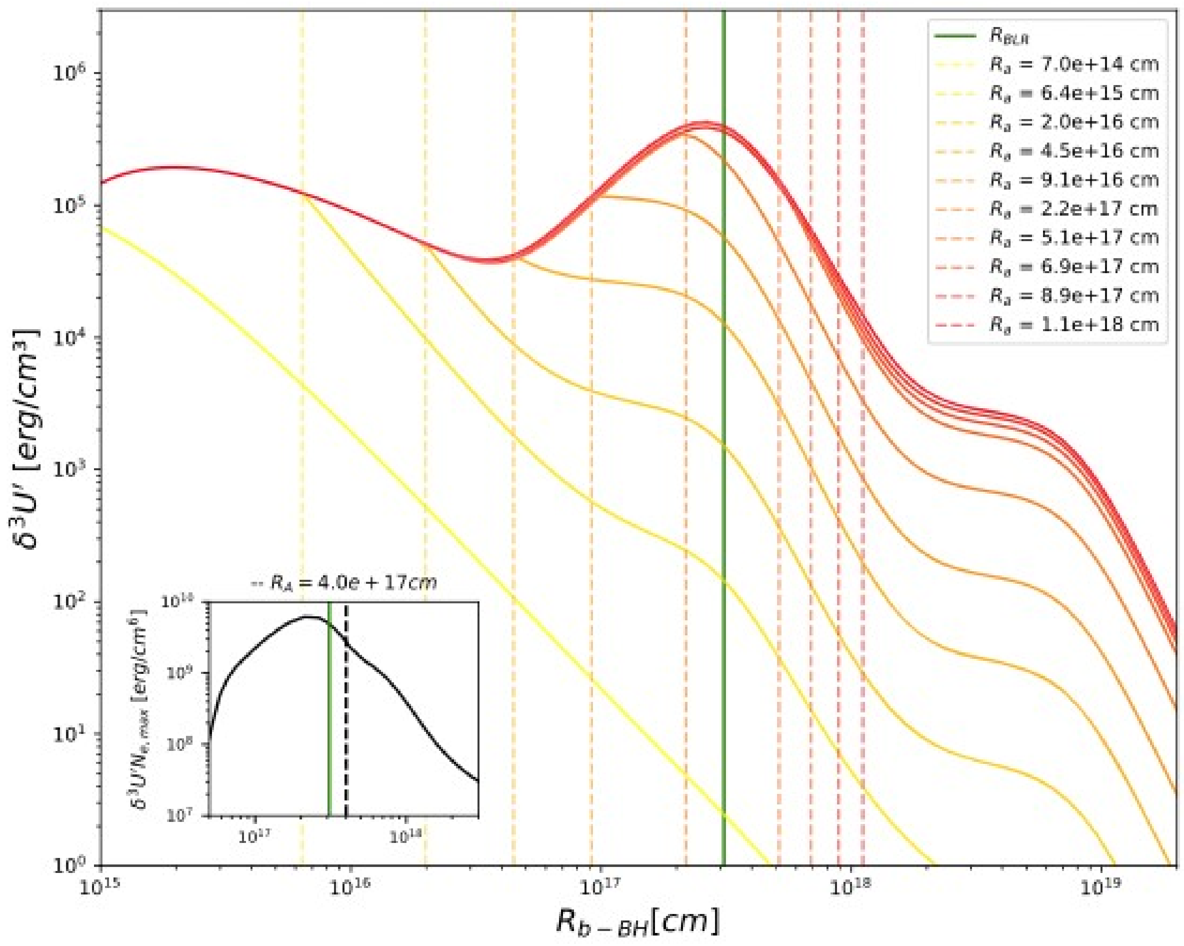

Comparison with observational constraints

Radio knots

Frequent observations of moving and accelerating knots in 3C 279

The resolved 230 GHz core region with the EHT (Kim et al., 2020) at de-projected distance along the jet of around 5 pc, i.e. >> our flaring blob 2. → no direct constraint

Jet acceleration region

VLBA : not clear whether the jet acceleration is completed on subparsec scales or continues at parsec scales and beyond (Homan et al., 2009). → compatible

ELT : Intrinsic acceleration region of the jet should be completed around 0.20 pc projected distance translating to around 6 pc along the jet from its base (Kim et al., 2020). → compatible

Bulk Lorentz factor

Observed Lorentz factors for individual components resolved with VLBI range from $\Gamma \sim 10 - 40$ (Bloom et al., 2013; Homan et al., 2009; Jorstad et al., 2017), while Lister et al. (2016) set the upper limit to $\Gamma \sim 50$.
→ compatible

Magnetic field strengths

Blob 1 :
Core-shift measurements based on VLBI data from the MOJAVE survey put the location of the radio core at 15.4 GHz at a distance of less than ~ 8 pc and its magnetic field strength at > 0.05 G.
B is limited to be < 0.42 G at a distance of 1 pc (Pushkarev et al., 2012).
The analysis of RadioAstron data by Toscano et al. (2025) yields a value of ~ 0.2 G near the 22 GHz radio core.

→ broadly consistent with our assumed magnetic field strength of 0.09 G for blob 1 at a distance of several parsec.

Blob 2 :
The problem : blob 2 should be in a magnetically dominated jet region, but has low magnetization and B-field !
A general problem in many leptonic blazar scenarios...

→ magnetic reconnection processes at play ?

→ injection of dense, unmagnetized material in the base of the jet ?

Application to other sources ?

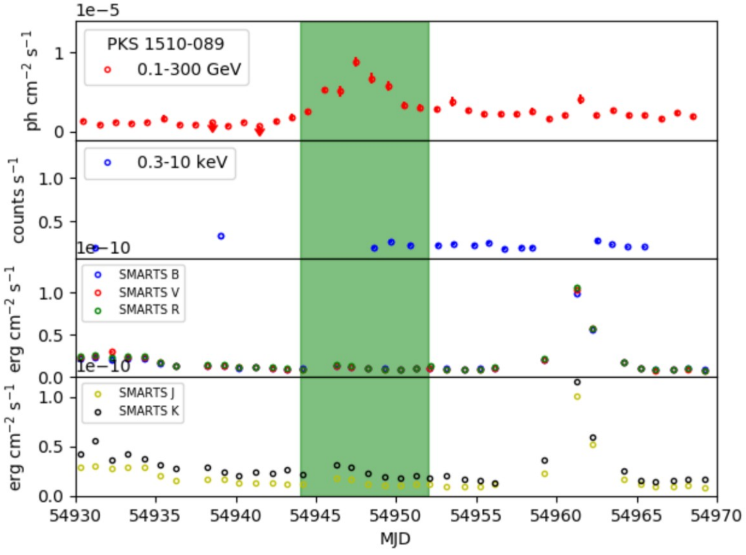

PKS 1510-089 , *Patel et al. 2021*

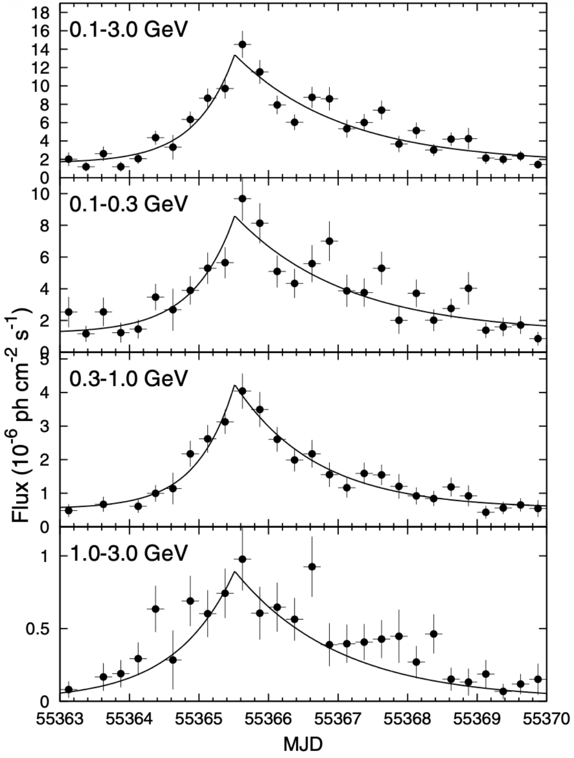

PKS 1222+216 ,
Kushwaha et al. 2014

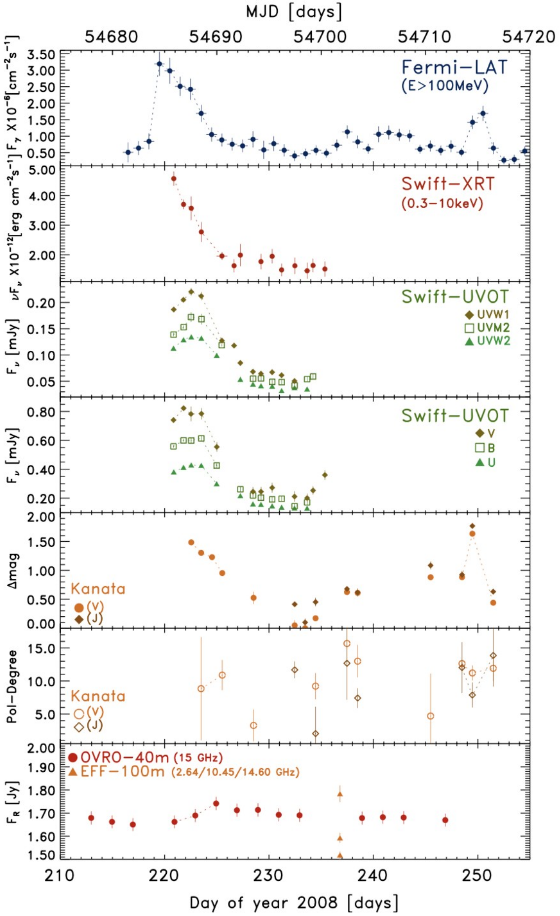

PKS 1502+106 ,
Abdo et al. 2010

light-curves for different acceleration mechanisms

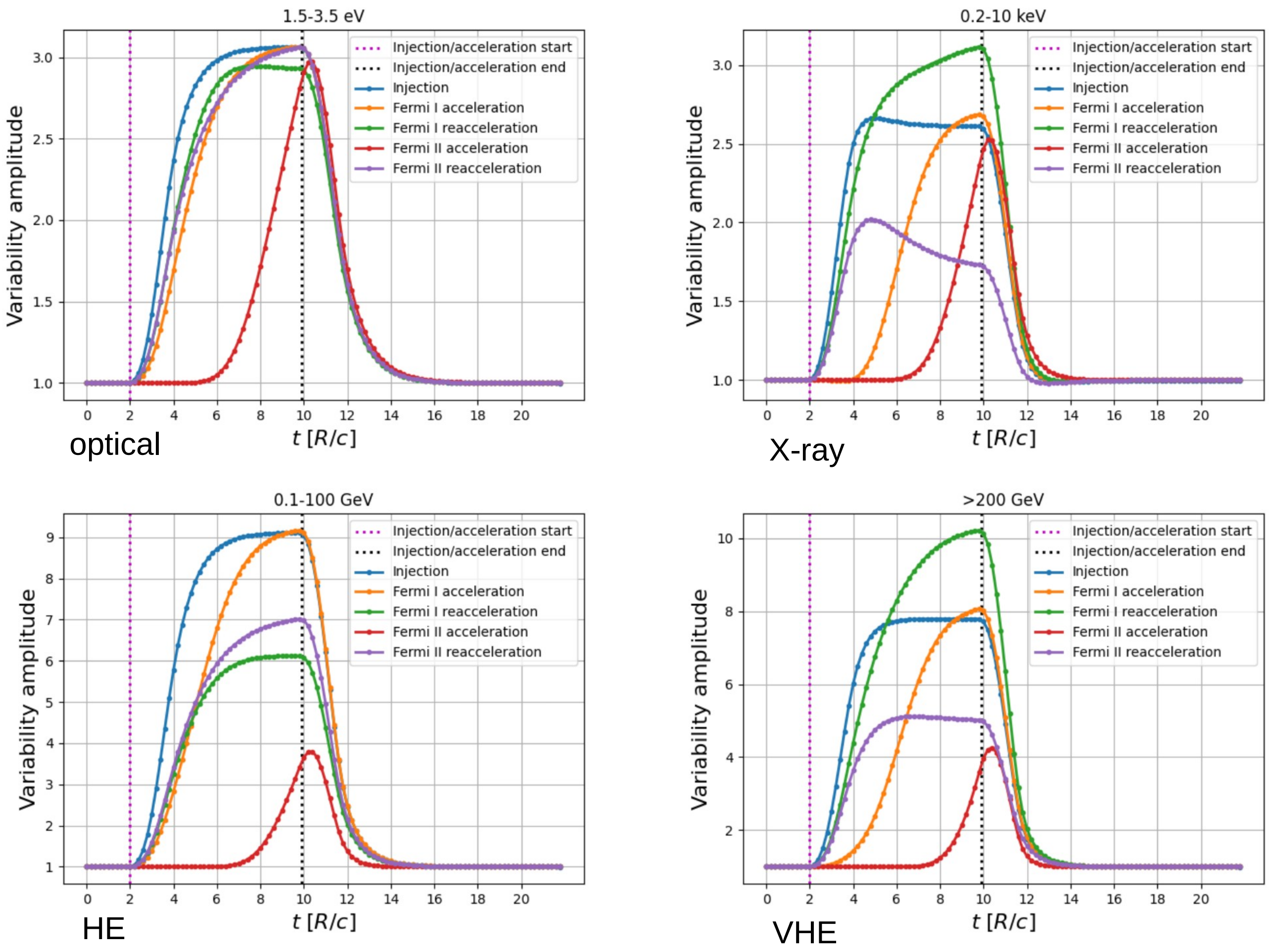

Comparison of different scenarios with same optical amplitude

Fermi I acceleration :

Delays between flare onset due to **gradual acceleration**.

Fermi II re-acceleration , Injection :

Flare peaks early in the X-ray band, then **IC cooling** sets in rapidly and leads to a flux decline.

Acceleration scenarios : parameters

Parameter	Variable	Value	Unit
Source			
Initial magnetic field	B_0	0.04	G
Magnetic field configuration	m_B	1	-
Initial blob radius	R_0	2.8×10^{16}	cm
Blob Doppler factor	δ	29	-
Redshift	z	0.0308	-
Angle to observer	θ	{0 ; 1}	°
Evolution			
Quiescent injection duration	$t_{\rm inj}$	30	R/c
Quiescent escape timescale	$t_{\rm esc}$	1	R/c
Beginning of expansion	$t_{\rm exp}$	0	R/c
Beginning of flaring	$t_{\rm flare}$	2	R/c
Duration of flaring	$t_{\rm dur}$	3	days*
Escape timescale during flaring	$t_{\rm esc,flare}$	1	R/c
Continuous injection spectrum			
Spectrum normalization	$\dot{N}_{\rm inj}$	1.86×10^{-14}	$cm^{-3}s^{-1}$
Spectrum slope	$\alpha_{\rm inj}$	-2.23	-
Pivot Lorentz factor	$\gamma_{\rm inj,pivot}$	1.0×10^5	-
Cutoff Lorentz factor	$\gamma_{\rm inj,cut}$	5.8×10^5	-
Minimal injected Lorentz factor	$\gamma_{\rm inj,min}$	800	-
Flaring injection spectrum			
Spectrum normalization	$\dot{N}_{\rm add}$	4×10^{-14}	$cm^{-3}s^{-1}$
Spectrum slope	$\alpha_{\rm add}$	-2.23	-
Pivot Lorentz factor	$\gamma_{\rm add,pivot}$	1.0×10^5	-
Cutoff Lorentz factor	$\gamma_{\rm add,cut}$	5.8×10^5	-
Minimal injected Lorentz factor	$\gamma_{\rm add,min}$	800	-
Particle acceleration			
Fermi I reacceleration timescale	$t_{\rm F_I}$	[0.7 – 2.0]	R/c
Turbulent spectrum slope	q	2	-
Maximum spectrum wavelength	$\lambda_{\rm max}$	[0 – 1]	R
Turbulence level	$\mathcal{L}_{\rm turb}$	[0 – 1]	-
Simulation grids			
Minimal electron Lorentz factor	$\gamma_{\rm min}$	100	-
Maximal electron Lorentz factor	$\gamma_{\rm max}$	1.0×10^7	-
Lorentz factor grid's points	n_γ	200	-
Simulation start time	$t_{\rm start}$	0	R/c
Simulation end time	$t_{\rm end}$	30	R/c
Time grid's bins	$n_{\rm bins}$	1000	-

The parameters for the injection scenario are: $R = 5.5 \times 10^{15}$ cm, $B = 0.2$ G, $\gamma_{\rm min} = 5 \times 10^3$, $\gamma_{\rm max} = 8 \times 10^5$. The same radius was used for the Fermi-I reacceleration scenario, but with a smaller magnetic field of $B = 0.05$ G and a smaller value of $\gamma_{\rm max} = 1.5 \times 10^6$ for the initial electron spectrum. Particle acceleration was achieved with an underlying weak turbulent acceleration ($\mathcal{L} = 0.4$, $\lambda_{\rm max} = 0.1$ R) and a dominant shock acceleration with timescale $t_{F_I} = 1.6$ R/c. The best scenario of Fermi-II reacceleration invoked a smaller radius of $R = 4.1 \times 10^{15}$ cm, an intermediate magnetic field strength $B = 0.1$ G, $\gamma_{\rm min} = 2 \times 10^3$ and $\gamma_{\rm max} = 2 \times 10^6$ for the initial injection. Particle acceleration during the flare was achieved with $\mathcal{L} = 0.6$ and $\lambda_{\rm max} = 0.1$ R.

blob moving through turbulent jet region

In this model using several zones, the continuous low-state emission from Mrk 421 is connected with a flare in Feb. 2010 :

- low state is modelled with a continuous injection (+ cooling, escape) of electrons accelerated on a bow shock

- the hard flare spectrum requires additional Fermi II acceleration from a turbulent emission region surrounding the blob as it passes through an inhomogeneous region inside the jet.

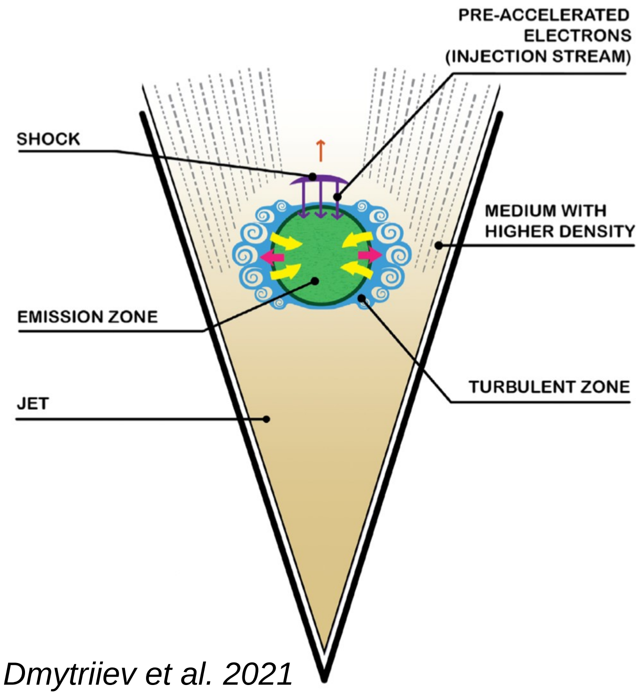

A. Dmytriiev et al. 2021

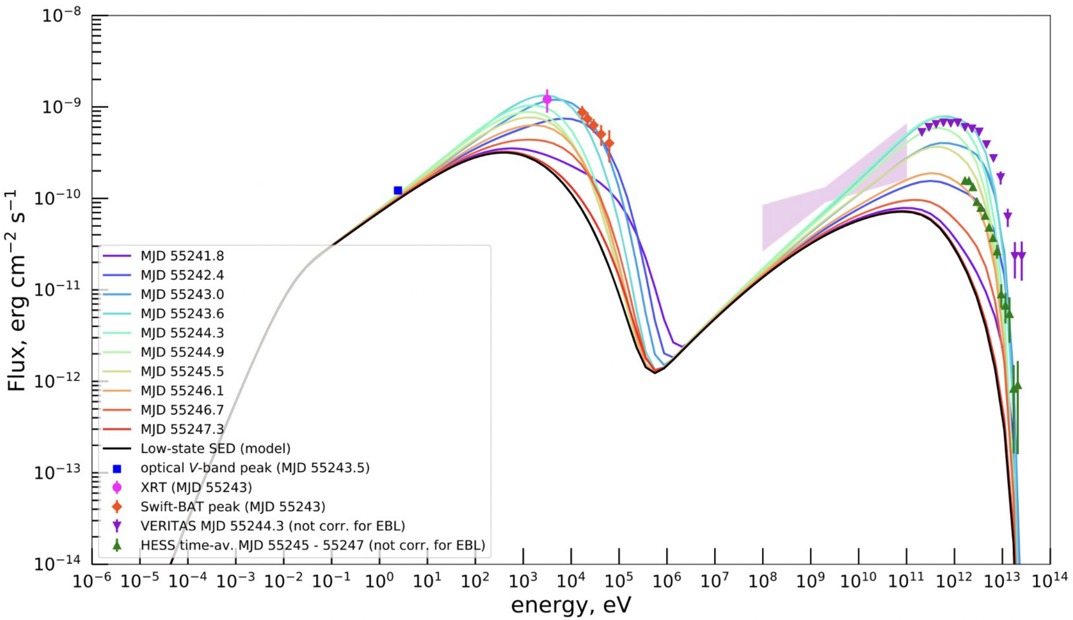

Broad-band emission from Mrk 421 during low state and flare + model curves.

blob moving through turbulent jet region

Time delays ?

HE band “synchronised” with **optical** band :
IC emission off optical photons

X-ray bands peak earlier than optical :
synchrotron emission from high-energy electrons with short cooling times

VHE bands peak a bit earlier than optical :
IC emission off higher energy photons

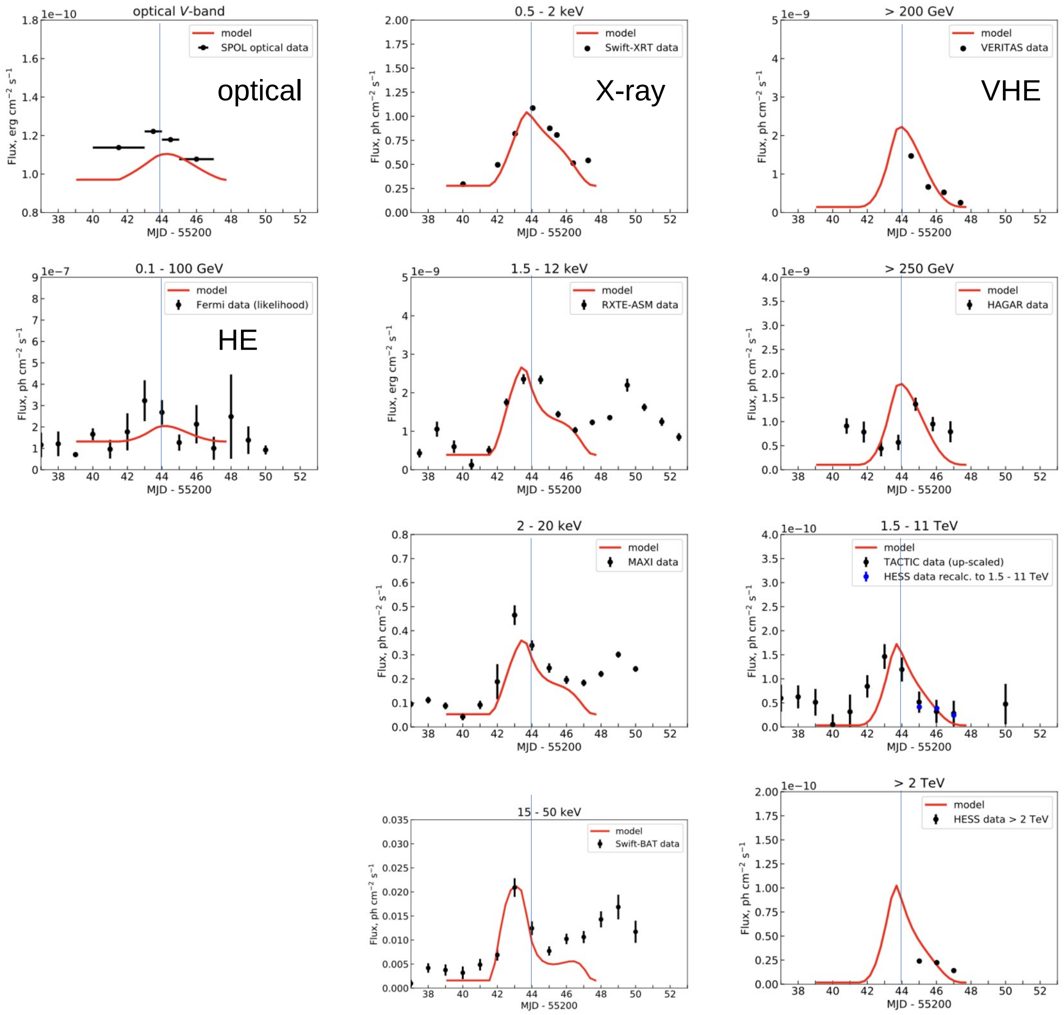

particle acceleration in jets

Possibly there is no single mechanism at play, but several mechanisms contribute in different regions of the jet.

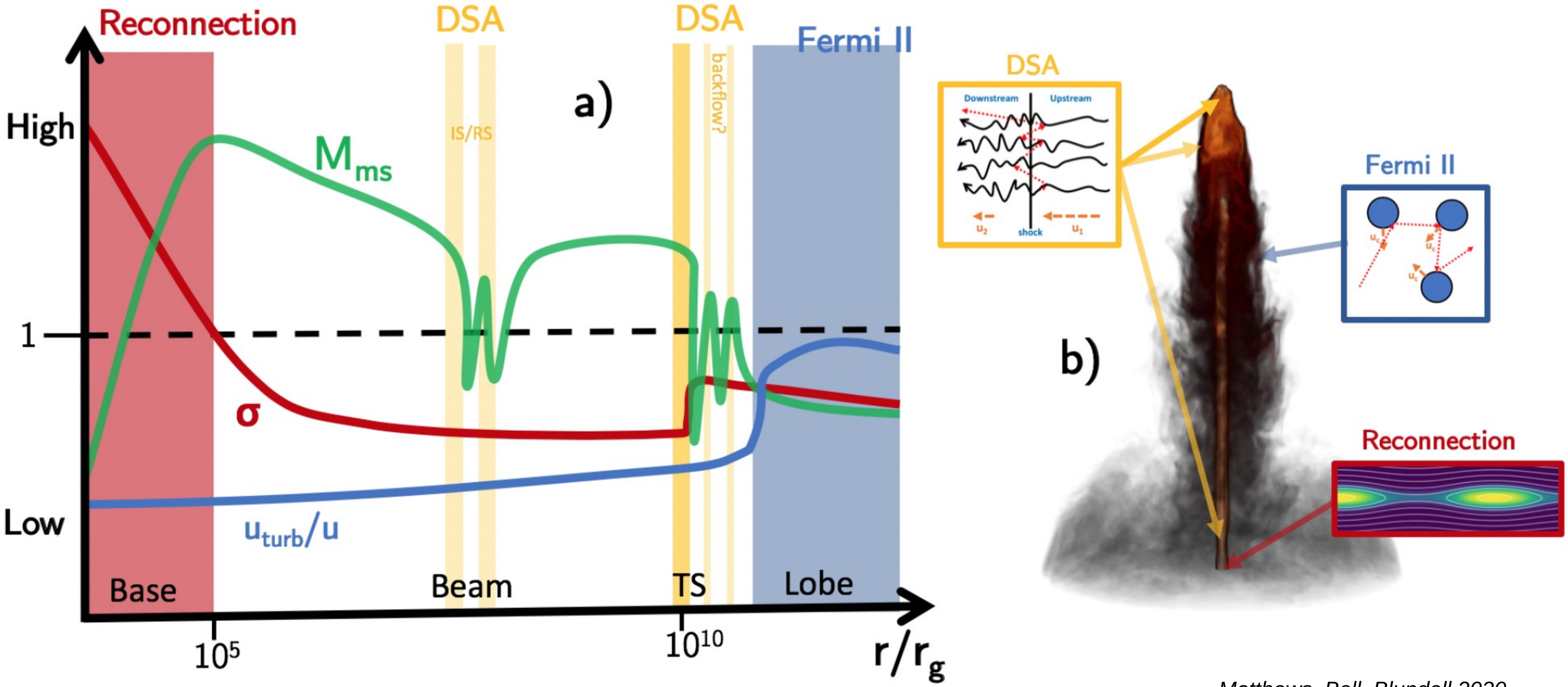

Matthews, Bell, Blundell 2020